CHARACTERIZATION OF LOW TEMPERATURE FERRITE/AUSTENITE TRANSFORMATIONS IN THE HEAT AFFECTED ZONE OF 2205 DUPLEX STAINLESS STEEL ARC WELDS

T.A. Palmer[1], J.W. Elmer[1], S.S. Babu[2], J.M. Vitek[2]

[1]Lawrence Livermore National Laboratory
Livermore, CA 94551, USA
[2]Oak Ridge National Laboratory, Oak Ridge, TN 37831 USA

Abstract

Spatially Resolved X-Ray Diffraction (SRXRD) has been used to identify a previously unobserved low temperature ferrite (δ)/austenite(γ) phase transformation in the heat affected zone (HAZ) of 2205 Duplex Stainless Steel (DSS) welds. In this "ferrite dip" transformation, the ferrite transforms to austenite in the weld HAZ at peak temperatures on the order of 750ºC. The austenite then re-transforms to ferrite during cooling, resulting in a ferrite volume fraction equivalent to that in the base metal. Time Resolved X-Ray Diffraction (TRXRD) and laser dilatometry measurements during Gleeble® thermal simulations are performed here in order to confirm the existence of this low temperature phase transformation. Experimental results, combined with thermodynamic and kinetic modeling of interstitial diffusion, have been used to investigate the mechanisms driving the "ferrite dip" transformation. These results indicate that the formation and decomposition of secondary austenite during heating and cooling, respectively, is most likely responsible for this observed behavior.

Introduction

The ferrite(δ)/austenite(γ) transformation in duplex stainless steels (DSS) during GTA welding has recently been monitored using an *in-situ* Spatially Resolved X-Ray Diffraction (SRXRD) technique.[1] In this study, x-ray diffraction is used to monitor the phases present at discrete locations in the weld Heat Affected Zone (HAZ). Based on these observations, the phase transformations occurring at locations across the length and width of the weld HAZ are identified. An analysis of the resulting x-ray diffraction patterns also provides a quantitative description of these phase transformations. Figure 1 shows the map of the measured ferrite volume fractions at discrete locations surrounding the weld pool.[1] The isotherms shown on the plot have been calculated using a well-tested three-dimensional thermo-fluids mathematical model.[2]

Using this map, the δ/γ phase transformations occurring in the HAZ during the weld heating and cooling cycles can be predicted as a function of both position and time. When coupled with the calculated thermal cycles, unique and previously unattainable kinetic information can be obtained, and a previously unobserved phase transformation is detected. Evidence for this transformation is shown in Figure 2, where the ferrite volume fractions measured at a location 9.5 mm from the weld centerline and corresponding thermal cycle are plotted. This unexpected low temperature transformation sequence is characterized by a decrease in the ferrite volume

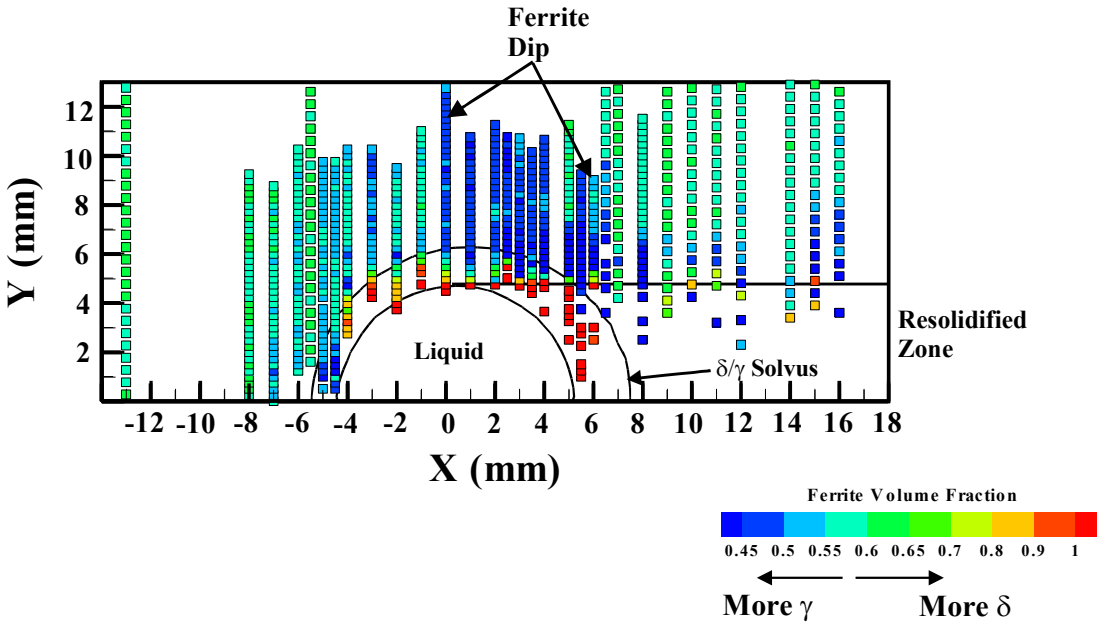

Figure 1. Phase map showing the δ volume fractions calculated from the SRXRD patterns. Two isotherms are shown, marking the liquidus temperature (1443ºC) and the δ/γ solvus (1316ºC) [1]

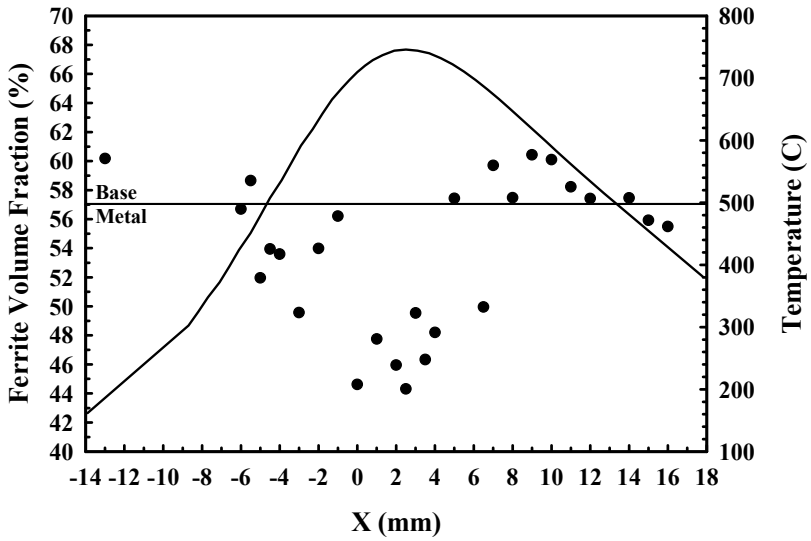

Figure 2. Plot showing variations in the temperature and the δ volume fraction with position, as measured during SRXRD experiments, relative to the heat source, at y=9.5 mm. A decrease of 10 to 15% is observed in the δ volume fraction during the heating portion of the thermal cycle, starting at a temperature of approximately 500˚C.

fraction on heating followed by a recovery of the ferrite volume fraction to its previous base metal value on cooling. This transformation sequence occurs at a peak temperature of approximately 750˚C with a heating rate of approximately 23˚C/sec and a cooling rate of approximately 15˚C/sec. Since the ferrite volume fractions return to the base metal value with the completion of this transformation, there is no evidence of this reaction having occurred in the post-weld microstructure. Therefore, only through the direct *in-situ* observation of the phase transformations using the SRXRD technique could this unexpected transformation be observed.

Over a similar temperature range (750˚C to 1000˚C), a number of other phase transformations have been characterized in 2205 and similar DSS alloys.[3-9] These transformations include the precipitation of intermetallic phases (i.e. σ, χ, R, and π) and carbides and nitrides during prolonged high temperature heat treatments or in the fusion zone during multi-pass welding. They are the primary result of alloy element partitioning, with Mo and Cr being two of the most important. The presence of these intermetallic phases, especially the σ phase, and the carbides and nitrides significantly degrade the corrosion resistance and mechanical properties of DSS alloys.

In addition to the precipitation of these secondary phases, the formation of austenite, with compositions different from the primary austenite formed at high temperatures in the as-received microstructure, has been reported.[3-9] A secondary austenite phase, which tends to have lower compositions of Cr, Mo, and N than the primary austenite, precedes the formation of other intermetallic phases during isothermal heat treatments between 750˚C and 1000˚C. Southwick and Honeycombe [10] have also postulated that an athermal martensitic-type process may also be responsible for the formation of austenite from ferrite at temperatures between 350˚C and 650˚C in their work on a 26% Cr-5% Ni stainless steel. The resulting austenite phase in this transformation has the same composition as the base metal ferrite phase.

The ferrite dip transformation sequence, first observed using SRXRD, will be further investigated and potential mechanisms for this transformation are examined. Additional experimental verification of this transformation sequence has been attempted. Time Resolved X-Ray Diffraction (TRXRD) experiments use synchrotron radiation to monitor phase transformations *in-situ* as a function of time at a single location in the HAZ of a spot weld. This technique is used to monitor the ferrite dip transformation sequence in a 2205 DSS spot weld in an attempt both to replicate the earlier findings in the SRXRD experiments and to directly monitor the transformation as a function of time. These results are then correlated with temperatures calculated at the individual monitoring locations. Radial dilatometry during Gleeble® thermal simulations, replicating the calculated thermal cycle in Figure 2, are also performed on base metal samples. This technique measures the expansion or contraction of the sample resulting from both thermal and any transformation strains occurring during this thermal cycle. Along with these experiments, results from the modeling of the thermodynamic stability and the kinetics of the δ/γ phase transformation are analyzed in an attempt to better understand the mechanisms governing the ferrite dip transformation sequence. Based on these experimental and modeling efforts, potential mechanisms for the transformation sequence, involving the formation of secondary austenite and a δ→γ transformation occurring by an athermal martensitic mechanism, are examined and discussed.

Experimental

Synchrotron-based X-Ray Diffraction Experiments

The TRXRD experiments are performed on the 31-pole wiggler beam line (BL 10-2) [11] at the Stanford Synchrotron Radiation Laboratory (SSRL) on the Stanford Positron-Electron Asymmetric Ring (SPEAR). In this setup, the synchrotron beam emerges from the wiggler and is focused by a toroidal mirror to a size of approximately 1 mm high x 2 mm wide and monochromated with a double Si(111) crystal. The focused beam then passes through a 540 μm tungsten pinhole to render a sub-millimeter beam on the sample at an incident angle of approximately 25˚. A schematic drawing of the basic features in the TRXRD experimental set-up is shown in Figure 3. This general set-up is similar to the SRXRD experiments and has been discussed extensively elsewhere.[12-18] Unlike the SRXRD experiments, though, the bar is not rotated beneath the fixed electrode here. In this case, a spot weld is made on the bar, and the x-ray is kept at a position a fixed distance from the welding electrode. During the spot welding process, 600

measurements are taken at 200 ms intervals, allowing the transformations to be tracked as a function of time.

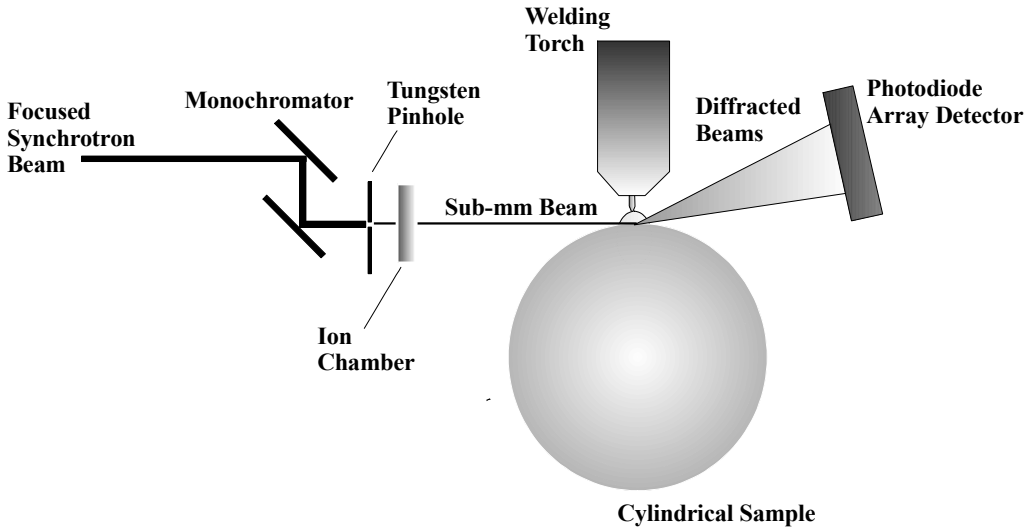

Figure 3. Schematic diagram of the TRXRD experimental set-up.

A photon energy of 12.0 keV (λ = 0.1033 nm) has been chosen to maximize the number of observable diffraction peaks and to ensure that the photon energy is high enough above the Fe (7.112 keV) and Ni (8.332 keV) K-edges to minimize the K-fluorescence contribution from the sample. TRXRD patterns are recorded using a 50 mm long, 2048 element position sensitive Si photodiode array detector. The detector array is Peltier-cooled and is placed approximately 10 cm from the x-ray incident point on the sample in order to cover a 2θ range from approximately 25˚ to 57˚, where θ is the Bragg angle. Within this 2θ range, there are three peaks associated with the bcc (δ-Fe) and three peaks associated with the fcc (γ-Fe) phases in the 2205 DSS.[19]

Gas tungsten arc (GTA) spot welds have been made on a cylindrical sample (10.2 cm diameter, 8 cm long) machined from commercial 2205 DSS forged bar stock (22.43 Cr-4.88 Ni-3.13 Mo-1.40 Mn-0.023 C-0.18 N-0.004 S-0.005 O-0.0007H-0.67 Si-0.02 Al-0.03 B-0.08 Co-0.20 Cu-0.03 Nb-0.028 P-<0.005 Ti-0.05 V- Bal. Fe). The as-received material has been solution annealed at 1065ºC for 2.5 hours followed by water quenching to ambient temperatures to give it nominally equal amounts of ferrite and austenite in the resulting microstructure. This material is the same alloy and heat used in the previously reported SRXRD experiments.[1]

These GTA spot welds are made using a peak current of 130 A and a background current of 90 A, pulsed at a frequency of 300 Hz. The pulsing parameters are designed to minimize the side-to-side motion of the liquid weld pool, thus decreasing the potential experimental error in the location of the liquid/solid interface. The arc gap is set at a distance of 0.28 cm, corresponding to an arc voltage of approximately 17 V, and welding is performed using a W-2% Th electrode with a diameter of 0.47 cm. Shielding is provided to the weld pool by high-purity (99.999%) helium being flowed through the torch and from a helium side blow, which removes soot (condensed metal vapors) from the area being examined with the synchrotron x-rays. The arc-on time for these experiments is set at 20 seconds. The welding process is monitored with an infrared (IR) camera (FLIR, Inc. Model SC1000). To avoid contamination of the weld metal with the external atmosphere, welding is performed in an environmentally sealed chamber. Prior to welding, the chamber is evacuated to a vacuum level of approximately 8 Pa using a mechanical roughing pump, after which the chamber is backfilled with helium until it reaches atmospheric pressure.

Analyses on the individual Bragg peaks in each TRXRD pattern are performed to measure their respective integrated intensity, full width at half maximum (FWHM), and 2θ values. Each experimental peak is fitted with a sum of one or more Gaussian peak profile functions and a linear background and then measured using an automated curve-fitting routine developed in Igor Pro®, Version 4.0. This technique is similar to one used to analyze SRXRD results.[1] Based on these measurements, important thermal and microstructural properties of various phases in the material at specific times can be extracted.

Additional analysis is performed on each diffraction pattern to estimate the ferrite and austenite volume fractions. These values are semi-quantitatively determined by measuring the respective integrated peak intensities for each phase and then calculating the ratio between these values and the sum of integrated intensities of all the peaks in the diffraction pattern. Since both phases are present at room temperature in the starting material, the intensity fractions are then normalized with respect to the base metal volume fractions measured using quantitative metallography. It is necessary to normalize the measured intensity fractions because of differences between the base metal δ/γ phase balance measured metallographically (54/46) and the base metal intensity fraction (62/38). A more in-depth description of this methodology is given elsewhere.[1]

Because of the many difficulties encountered in the accurate measurement of temperatures in the spot weld HAZ, a transient numerical heat transfer and fluid flow model, developed by previous researchers,[2] is used to calculate the thermal cycles experienced here. Extensive testing on this material system [1] and other materials systems, including C-Mn steels [2,20-21] and titanium [16] has been performed, providing verification for the model. In this model, the governing equations are solved in a three dimensional Cartesian coordinate system. A computation time of 60 seconds is used; allowing the cooling cycle to be monitored for 40 seconds after the arc is extinguished. The material parameters used in these calculations are shown in Table I.

Table I Material And Numerical Scheme Parameters Used In The Spot Weld Model.

Property	Value	Reference
Liquidus Temperature (K)	1715	*
Solidus Temperature (K)	1589	*
Density of Liquid (kg/m^3)	7200	22**
Enthalpy of Solid at Melting Point (J/kg)	1.05×10^6	23
Enthalpy of Liquid at Melting Point (J/kg)	1.32×10^6	23
Specific Heat of Solid (J/kg-K)	418.68	22
Specific Heat of Liquid (J/kg-K)	808.05	22
Thermal Conductivity of Solid (W/m-K)	18.83	22**
Thermal Conductivity of Liquid (W/m-K)	41.84	22**
Viscosity of Liquid (kg/m-sec)	0.0085	22
Temperature Coefficient of Surface Tension (N/m-K)	-9.25×10^{-4}	22**
Coefficient of Thermal Expansion (1/K)	1.00×10^{-5}	22
Arc Radius (cm)	0.275	
Arc Efficiency (%)	40	
Time Step (sec)	0.01	
Arc On Time (sec)	20	

* Values are based on calculations provided by ThermoCalc for an alloy of this composition.
** Values are based on approximations from pure metal values.

The calculated spot weld dimensions and those measured in a typical weld cross section show good agreement. For example, the measured diameter of the top surface (10.48±0.51 mm) compares well with the value calculated using the thermo-fluids model (10.60 mm). The measured cross section depth of the spot weld (1.72 mm) also compares favorably with the calculated value (1.92 mm). Even though there is a difference between the measured and calculated weld pool dimensions, the difference in dimensions is small enough that the resulting thermal cycles at the monitoring location are minimal.

The initial heating and cooling rates, calculated immediately after the initiation and extinguishing of the arc, are extremely rapid, especially at locations closest to the heat source. For example, the heating and cooling rates directly underneath the heat source are 780ºC/sec and 505ºC/sec, respectively, for two-second periods immediately following the initiation and extinguishing of the arc. As the distance from the fusion zone center is increased, the calculated heating and cooling rates decrease. In particular, at a location 3 mm from the fusion zone boundary, which corresponds with where the TRXRD measurements are made, the heating and cooling rates at these same times are 129.8ºC/sec and 127.6ºC/sec, respectively. After the initially rapid heating and cooling, these rates slow considerably.

Gleeble® Thermal Simulations

Thermal simulations, replicating those calculated in the 2205 DSS GTA weld HAZ during SRXRD experiments,[1] have been performed on a Gleeble® 3500 Thermo-mechanical Simulator. The Gleeble® samples, which are rods approximately 6.35 mm in diameter and 76.2 mm in length, have been removed from the as-received forged bar at an orientation parallel to the extrusion direction. The accompanying microstructural orientation of the as-received bar is shown in Figure 4. In this figure, the austenite phase, which is the lighter colored of the two phases, can be characterized as generally having a rod-like morphology, with the rods oriented parallel to the extrusion direction of the bar.

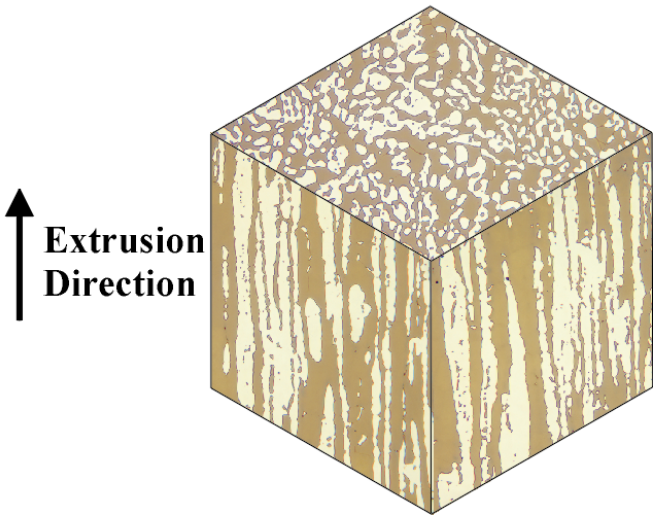

Figure 4. Three dimensional representation of microstructural orientation of the as-received 2205 DSS base metal.

Each sample is heated from room temperature to 740°C at a heating rate of 30°C/s. It is then held at this temperature for 4 seconds to achieve thermal equilibrium before cooling and is then cooled to room temperature at a cooling rate of 15°C/s. The transformation strains are measured radially using a non-contact laser dilatometer. The sample is initially loaded in a random rotation with reference to the extrusion axis (0° measurement), and the dilatations resulting from the applied thermal cycle are then measured. After these measurements are completed,

the sample is precisely rotated to 45° from its original position, and the thermal cycles are repeated (45° measurement). Finally, the sample is rotated another 45°, and another set of measurements are taken during the same thermal cycle (90° measurement).

Results

Synchrotron-based X-Ray Diffraction Experiments

A TRXRD run has been performed by positioning the beam approximately 8 mm from the center of a spot weld, which corresponds to a distance of 3 mm from the final fusion zone boundary with an arc on time of 20 seconds. Figure 5 shows the pseudo-color plot of the 2θ values vs. time for this TRXRD run. This figure shows only the portion of the 2θ range with the fcc(111), bcc(110), and fcc(220) peaks. Outside this 2θ range, there is little change in the observed peak properties. Ferrite and austenite peaks appear throughout the heating and cooling cycles. The peak intensities for the prominent fcc(111) and bcc(110) change very little over the course of the run, except in the region immediately preceding and following the extinguishing of the arc. Here, the fcc(111) peak intensity increases at times preceding the end of the heating cycle but returns to previous levels as the cooling cycle begins.

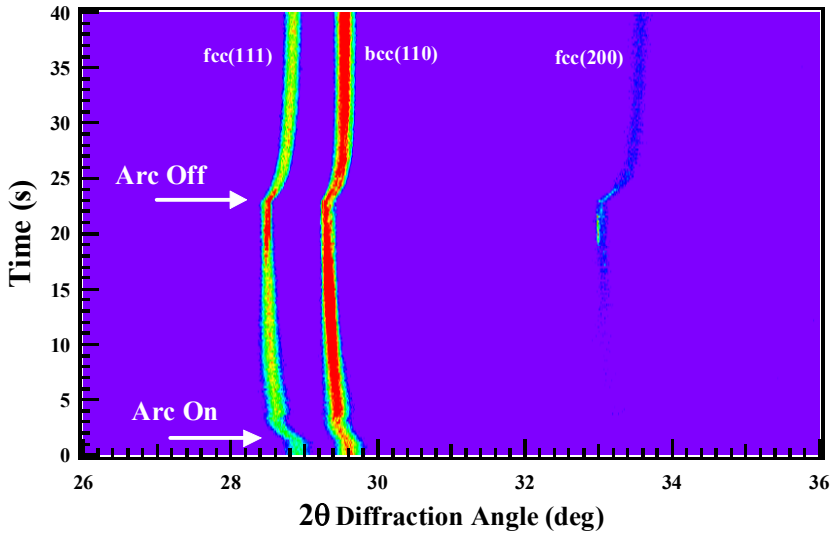

Figure 5. Plot showing variations in peak intensities over the course of the TRXRD run.

Since the base metal microstructure in this alloy is textured, an analysis of the peaks detected at each time can only be considered to be semi-quantitative in nature. Here, it is assumed that the integrated intensities of the peaks in each diffraction pattern can be converted to ferrite volume fractions. These date are plotted in Figure 6, along with the calculated thermal cycle, as a function of time. In this plot, three distinct transformation regions (ferrite growth, dip, and recovery) are identified. The calculated thermal cycle displays a peak temperature of approximately 720ºC, with a heating rate of approximately 35ºC/sec, which is calculated over the course of the entire heating cycle, and a cooling rate of approximately 128ºC/sec, which is calculated over the first two seconds of cooling. The observed decrease in the ferrite volume fraction at the latter stages of the heating cycle and the recovery of the ferrite volume fraction at the initiation of cooling are similar to what is observed in the SRXRD experiments and indicate that some type of transformation is taking place.

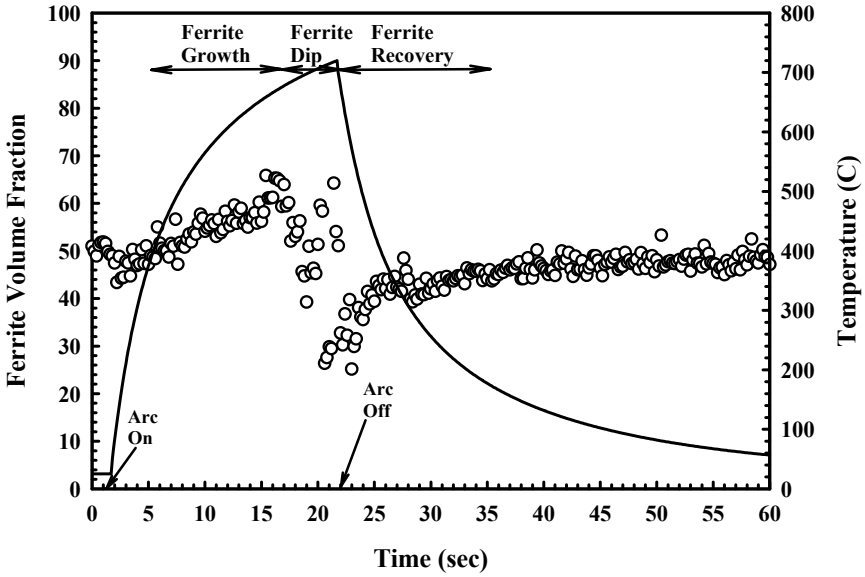

Figure 6. Plot showing the measured ferrite volume fraction and the calculated thermal cycle for the TRXRD run. Regions of the ferrite growth, dip, and recovery are shown.

Characteristics of the individual peaks are also measured and are summarized in Table II. Here, the times, temperatures, ferrite volume fractions, lattice parameters, and FWHM values associated with each transformation region over the course of the TRXRD run are listed. Particular attention, though, is given to shifts in the 2θ and FWHM values for the fcc(111) and bcc(110) peaks, which are plotted in Figures 7 and 8, respectively. In general, the decrease in the 2θ values observed during heating in Figure 7 relates to the expansion of the lattice, while the increase in the 2θ values corresponds to lattice contraction during cooling. Because of its higher coefficient of thermal expansion, the 2θ shift for the fcc phase is greater than that for the bcc phase. The data included in this plot also provide evidence of any strains resulting from phase transformations occurring at this location.

Table II Characteristics of the ferrite growth/dip/recovery transformation sequence.

	Original	**Ferrite Growth**		**Ferrite Dip**		**Ferrite Recovery**		**Final**
		Start	End	Start	End	Start	End	
Time (sec)								
	0	3	16.2	17	23	23.2	35.2	120
Temperature (ºC)								
	25	232	671	680	720	687	173	----
Ferrite Volume Fraction								
	49.42	47.82	65.28	63.93	25.17	29.91	46.02	51.60
Lattice Parameter (Å)								
Austenite	3.576	3.613	3.631	3.633	3.633	3.630	3.587	3.581
Ferrite	2.862	2.876	2.887	2.888	2.893	2.886	2.869	2.869
FWHM								
fcc(111)	0.2062	0.1647	0.0988	0.0960	0.0594	0.0569	0.1057	0.1981
bcc(110)	0.1981	0.1645	0.0766	0.0838	0.0943	0.0928	0.1165	0.1303

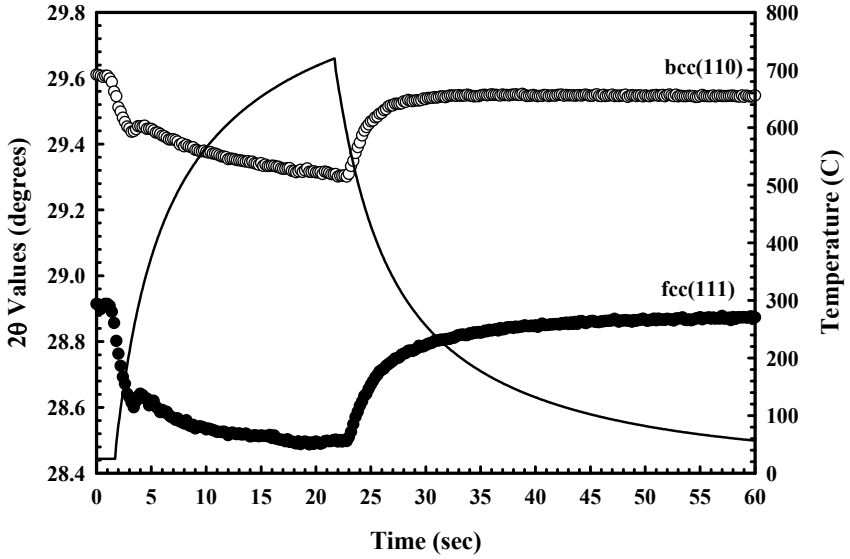

Figure 7. Plots showing the variation in the 2θ values for the fcc(111) and bcc(110) for the TRXRD run.

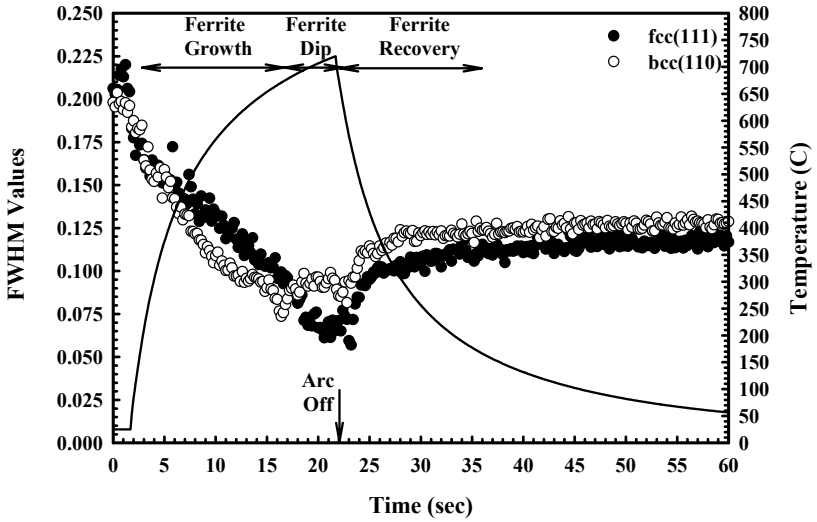

Figure 8. Plot showing the variation in the FWHM values for the fcc(111) and bcc(110) peaks for the TRXRD run. Regions of the ferrite growth, dip, and recovery are shown.

Changes in the FWHM values of individual peaks, which are plotted in Figure 8 as a function of time for the bcc(110) and fcc(111) peaks also provide additional useful information. An increase in these values generally corresponds to an increase in the micro-strain in a particular phase. In the SRXRD experiments, a narrowing of the peak width is used to denote the onset of annealing of both ferrite and austenite at elevated temperatures.[1] In this plot, both peaks exhibit a narrowing during the heating cycle and a broadening during the cooling cycle. However, in the "ferrite dip" region, coinciding with the drop in the ferrite volume fraction, the FWHM values for only the bcc(110) peak increase, which is the opposite behavior than that expected during heating. Such an increase in the peak width points to a non-uniform microstrain developing in the ferrite phase.[24] The formation of such a microstrain may be caused by the initiation of a phase transformation. At the conclusion of the TRXRD run, the FWHM values for both peaks are smaller than those in the as-received condition. The resulting microstructure, therefore, exists in a different stress state than the as-received microstructure, even though the ferrite volume fraction is essentially unchanged. These results are consistent with annealing of

the microstructure, which has been shown to occur at temperatures above approximately 550ºC in this alloy system.[1]

Gleeble® Thermal Simulations

Laser dilatometry measurements have been made on 2205 DSS samples subjected to a thermal cycle similar to that shown in Figure 2 in an attempt to detect the low-temperature phase transformation observed during both SRXRD and TRXRD experiments. The samples are machined from the as-received bar along an orientation parallel to the extrusion direction, making the longitudinal direction of the bar perpendicular to the incident orientation of the x-rays. This material orientation matches that in the synchrotron based x-ray experiments. Since the ferrite and austenite volume fractions are changing in ratio with each other during heating and the CTE of each phase is different, a rather complex dilatometric response is expected during testing. With such complex results, further analysis of the resulting curves is required.

The dilatometric results from the three orientations are shown in Figure 9, along with a small schematic figure showing these general orientations. In this plot, the data for each orientation show a systematic trend, dominated by a continuous change in the slope over the applied temperature range. On the other hand, a closer examination of the curves reveals a difference in the measured slopes at lower and higher temperatures. For example, in the 45º orientation, the slope of the curve from 25ºC to 400ºC is approximately 1.464×10^{-5}/ºC, and from 400ºC to 740ºC, the slope of the curve changes to 1.704×10^{-5}/ºC. Most importantly, the slope changes again between 600ºC and 740ºC to 1.837×10^{-5}/ºC. The change in slope, especially at the higher temperatures, corresponds with the "ferrite dip" transformation.

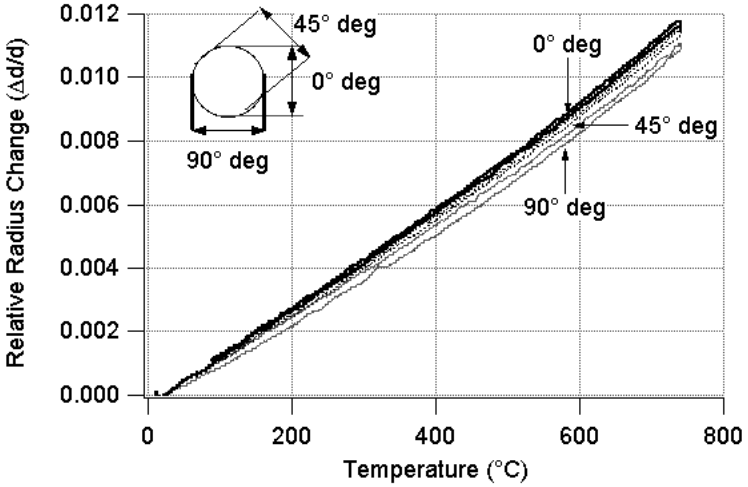

Figure 9. Plots showing the dilatometric results for a 2205 DSS sample at three different orientations.

The measured relative diameter changes are not identical in each orientation, indicating that there is an orientation-specific nature to the dilatometric response of the alloy. This orientation dependence most likely corresponds to the effects of microstructural texturing in the alloy, which is displayed in the base metal microstructure shown in Figure 4. The dilation curves also show that the sample exhibits no net plastic strain after each thermal cycle, indicating that the behavior may be reversible. In the range of temperatures where the ferrite dip and recovery transformations are identified in the TRXRD and SRXRD experiments, no obvious dip in the dilatometric strain of the sample is observed. However, since two phases are expanding at different rates, and since the phase transformation may be occurring simultaneously, the dip may

be difficult to detect. More work is required in the analysis of this dilatometric data in order to separate the effects of thermal expansion and the observed phase transformations.

Phase Transformation Modeling Overview

A series of calculations have recently been performed to evaluate the kinetics of the "ferrite dip" transformation,[25] based on the assumption that diffusion controls the phase transformation. Both ortho-equilibrium and para-equilibrium conditions at the δ/γ interface are considered. In the ortho-equilibrium calculations, which are performed using the Dictra software[26], equilibrium is assumed at the interface between ferrite and austenite for the Fe-Cr-Ni-C-N system, with a partitioning of all alloying elements similar to that observed in the base metal. The equilibrium interface condition establishes compositional gradients near the interface and the resultant diffusion controls the transformation behavior. In all cases, the model calculations show that the transformation behavior is very sluggish at the temperatures experienced in the weld HAZ. In order to achieve significant changes in ferrite levels in the time frame corresponding to the SRXRD measurements, temperatures on the order of 1100°C are needed for the transformation to proceed. These temperatures are well in excess of the peak temperatures observed in the weld HAZ during TRXRD and SRXRD experiments.

Diffusion controlled growth has also been modeled using a para-equilibrium interface condition. MatCalc software [27] has been used to perform these calculations with only the diffusion of N being considered. Since the diffusion rate of nitrogen is much higher than that of the substitutional alloying elements considered previously, these simulations show that ferrite dissolution and re-formation can take place over times frames similar to welding. During the heating cycle, the ferrite fraction is shown to decrease. Upon cooling, the ferrite fraction is shown to increase and nearly reaches the initial ferrite fraction value, corresponding to the recovery in the ferrite volume fraction observed in the SRXRD experiments. The extent of ferrite dissolution during heating and ferrite re-formation during cooling is roughly the same as that observed by SRXRD. The same results are found when actual N contents, as well as when elevated N contents, combining both the carbon and nitrogen levels, are used. However, the calculations show that the ferrite dissolution during heating is more rapid than the ferrite formation during cooling, which is the reverse of that observed in the SRXRD experiments. Nonetheless, these calculations provide evidence for the possible role of nitrogen in this transformation.

Discussion

Both TRXRD experiments and laser dilatometry during Gleeble® thermal simulations have been performed in an attempt to replicate the "ferrite dip" transformation observed during the SRXRD experiments.[1] Based on the observations described above, the existence of the previously observed "ferrite dip" transformation has been confirmed. However, questions regarding the mechanisms responsible for this transformation have not been satisfactorily answered by these experiments alone. It is therefore necessary to combine both the existing experimental and modeling work in an attempt to consider other mechanisms.

An analysis of the calculated thermodynamic stability of the ferrite and austenite phases in this alloy has been performed using ThermoCalc®, with the precipitation of intermetallic phases, such as σ and χ, being suppressed. The results of this analysis are shown in Figure 10, which includes the base metal heat treatment conditions and resulting δ/γ fractions indicated on the plot. In the as-received condition, the ferrite and austenite volume fractions exist in a metastable state because the alloy is heat treated at approximately 1065ºC before being quenched to room temperature. Therefore, the resulting δ/γ fractions are more in line with what is expected at higher temperatures than at room temperature. These theoretical base metal values and those observed metallographically in the as-received material compare favorably. There is also

clearly a thermodynamic basis for the observed ferrite dip. The plot shows the presence of a dip in the ferrite content, which reaches a minimum value at about 860ºC.

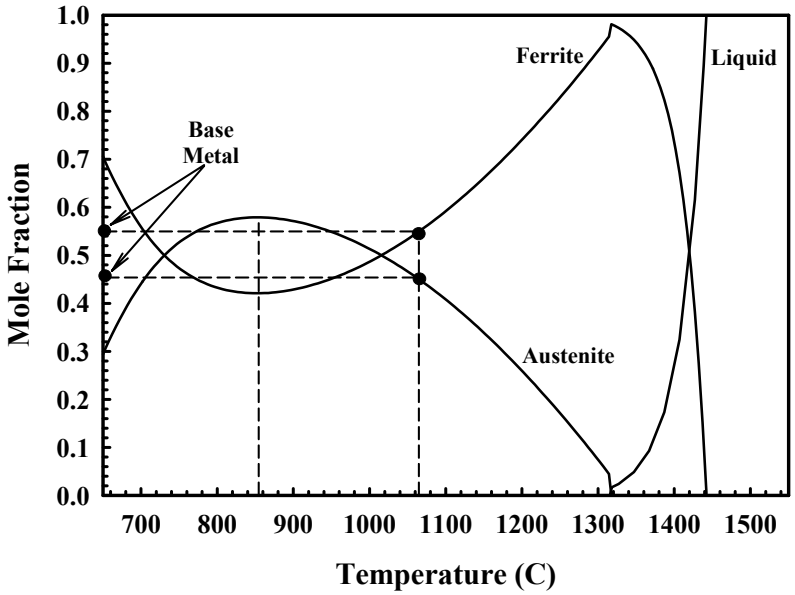

Figure 10. Plot showing equilibrium thermodynamic calculations, using ThermoCalc®, of the stability of the ferrite, austenite, and liquid phases in the 2205 Duplex Stainless Steel analyzed here. The base metal solution treating temperature (1065ºC) and resulting ferrite and austenite fractions are indicated on the plot.

The kinetics of the ferrite dip and recovery transformations are also measured in both the SRXRD and TRXRD experiments in terms of the rates of change of the ferrite volume fraction as a function of time. During the SRXRD experiments [1], similar heating and cooling rates produce similar rates of change in the ferrite volume fractions during the dip and recovery (1.08 vol.% δ/sec and 1.49 vol.% δ/sec). These values, though, are much lower than those recorded in the TRXRD results (6.46 vol.% δ/sec and 5.07 vol.% δ/sec), which are produced at much slower heating (7ºC/sec) and more rapid cooling (55ºC/sec) rates over the times during which the ferrite dip and recovery are observed.

Even though significant differences exist between the two sets of results, they can be traced, at least in part, to differences in the overall thermal cycles experienced in each experiment. In the SRXRD experiments, the similar rates in the ferrite dip and recovery are produced by nearly equivalent heating and cooling rates. On the other hand, the heating rate in the TRXRD experiments is significantly lower in magnitude than the cooling rate. Yet, similar rates of change in the ferrite volume fractions during the ferrite dip and recovery are observed. These rates are also significantly higher than those observed in the SRXRD experiments. The role of diffusion, especially that of nitrogen, in these transformations is bolstered by this difference in rates with different applied thermal cycles. The TRXRD experimental observations show, as well, that the ferrite dip is slightly more rapid than the ferrite recovery, corresponding with the para-equilibrium modeling of nitrogen diffusion in this alloy.[25]

A more in-depth analysis of the new TRXRD experimental data may prove worthwhile in obtaining a better understanding of this phenomenon. Evidence of the governing mechanisms for this transformation may be present in the shifts in the peak positions and the peak widths in the TRXRD experiments. These changes in the peak characteristics are summarized in Table II, where the results are divided into the three regions of the “ferrite dip” transformation sequence. In the table, the lattice parameters for the ferrite and austenite phases, which are calculated from

the 2θ values of each peak present in the selected diffraction patterns using Bragg's Law, are listed.

As shown in Table II, the expansion and contraction of the austenite lattice parameters in the ferrite growth and recovery regions is greater than that for the ferrite phase. These values are expected, given the higher coefficient of thermal expansion for austenite. However, over the course of the ferrite dip region, the austenite lattice parameter shows no change and maintains nearly the same value as that observed at the end of the ferrite growth region. The ferrite phase, though, displays a slight expansion in the ferrite dip region, providing an indication of differences in the behavior of the two phases under these conditions. The FWHM values for the bcc(110) peaks, shown in both Table II and Figure 8, display a variation in their expected behavior in the ferrite dip region as well. This unexpected disparity is an indication that the phases are reacting differently, and that the micro-stress state of ferrite, in particular, is behaving in a way opposite to that which would be expected with heating alone.

Based on these results, it appears that the diffusion of nitrogen may play a role in driving these transformations, but the results are not definitive. Therefore, the formation of secondary austenite and a low temperature martensitic transformation of ferrite to austenite, both previously observed by other researchers [3-10], are discussed as potential mechanisms. In the case of secondary austenite formation, the general temperature range over which it has been observed (750ºC to 1000ºC) matches that observed experimentally for the decrease in ferrite volume fraction observed during heating. The secondary austenite phase contains lower amounts of key alloying elements than the primary austenite in the base metal, which have been the basis for the previous kinetic and thermodynamic calculations.[25]

Thermodynamic calculations modeling the formation of secondary austenite have shown that the formation of secondary austenite is possible when considering para-equilibrium of nitrogen between primary austenite and ferrite.[5] If diffusion is the controlling mechanism, then the transformation must occur in a region where the diffusion distances are small, which is most likely at the ferrite/austenite boundary. As a result of the heat treating and quenching that this alloy has undergone, the alloying elements are not evenly divided between the phases. In particular, nitrogen is partitioned to the austenite phase,[25] thus providing a potential driving force for the diffusion of nitrogen between the two phases. The diffusion of nitrogen between ferrite and austenite may occur, since the austenite and ferrite in the base metal are metastable, due to the solution anneal and quench from1065ºC.

Secondary austenite in typical DSS alloys has been observed in the resulting microstructure after a variety of isothermal heat treatments of varying durations.[5-9] Therefore, under these conditions, the ferrite recovery portion of the ferrite dip transformation sequence has gone unobserved. In order for the ferrite volume fraction to return to its as-received levels, the nitrogen, which diffused into the ferrite to drive the initial transformation, must diffuse back into the austenite during cooling. A dip in the ferrite stability is predicted in this same temperature range by equilibrium thermodynamic calculations (Figure 10), providing a theoretical basis for these experimental observations.

The potential for a low temperature martensitic-type transformation of ferrite to austenite, like that reported by Southwick and Honeycombe [10], is also under consideration. Since the austenite resulting from this transformation possesses the same composition as the ferrite phase, no diffusion is required. Such a diffusionless transformation would be supported, in part, by the previous modeling work [25], in which the times and temperatures present in the SRXRD experiments are not high enough to drive the diffusion of substitutional alloying elements. In addition, the austenite resulting from such a martensitic transformation would be highly strained compared to the primary austenite and ferrite, and changes in the peak characteristics would be expected. Such changes, primarily in the FWHM values for the ferrite phase and the shift in the

fcc(111) peak at the initiation of the ferrite dip transformation are potential indications of these changes. With no diffusion involved and the transformed austenite having the same composition as the ferrite, the back-transformation to ferrite with cooling can also be described, like the case for secondary austenite formation and decomposition, using the increasing stability of ferrite at lower temperatures, which is shown in Figure 10.

Summary And Conclusions

The ferrite dip transformation sequence, characterized by a decrease in the ferrite volume fraction during heating to peak temperatures of approximately 750ºC, followed by a recovery of ferrite to base metal levels during cooling has been first observed during SRXRD experiments. Both TRXRD experiments and laser dilatometry in Gleeble® thermal simulations have been performed in an attempt to verify this behavior. A summary of the experimental findings is given below:

- TRXRD experiments coupled with calculated thermal cycles show the ferrite dip occurring over the course of a thermal cycle similar to that previously observed during SRXRD experiments.
- In the TRXRD experiment, the rate of change in the ferrite volume fractions during the ferrite dip as a function of time exceeds that observed during the recovery. These observed trends correspond with those determined during the para-equilibrium modeling of nitrogen diffusion in this alloy system.[25]
- An analysis of the peak characteristics from the TRXRD experiment shows that at the initiation of the ferrite dip there is a noticeable broadening of the ferrite peaks. Changes in the peak characteristics provide an indication for the role of diffusion in driving these differences in the behavior of each phase as the ferrite dip and recovery transformations proceed.
- Laser dilatometry during Gleeble® weld thermal simulations has been performed on 2205 DSS base metal samples at different orientations. The results show differences in both the measured dilations, indicating that there is an orientation-specific nature to the transformation observed here. This orientation dependence most likely corresponds to the effects of microstructural texturing in the alloy.

Two potential mechanisms for the ferrite dip transformation sequence are examined: the formation of secondary austenite and an athermal martensitic-type transformation of ferrite to austenite. Of these two mechanisms, the formation and decomposition of secondary austenite present the most likely scenario. Further work is required in order to definitively identify the mechanism responsible for this observed phase transformation. Regions in the HAZ where this transformation is observed should be examined using Transmission Electron Microscopy (TEM) in order to provide direct evidence for the dominant mechanism at the high resolutions required.

Acknowledgments

This work has been performed under the auspices of the U.S. Department of Energy, by the University of California, Lawrence Livermore National Laboratory under Contract No. W-7405-ENG-48. Portions of this research were carried out at the Stanford Synchrotron Radiation Laboratory, a national user facility operated by Stanford University on behalf of the U.S. Department of Energy, Office of Basic Energy Sciences. The ORNL portion of this research was sponsored by the U. S. Department of Energy, Division of Materials Science and Engineering,

under contract DE-AC05-00OR22725 with UT-Battelle, LLC. The authors would also like to thank Prof. T. DebRoy at The Pennsylvania State University for allowing us the use of the transient heat transfer and fluid flow code for the calculation of weld thermal cycles. Other thanks go to Mr. A.T. Teruya (Lawrence Livermore National Laboratory) for writing the LabView® software used in the control of the welding experiments.

References

1. T.A. Palmer, J.W. Elmer, and J. Wong, "*In-Situ* Observations of Ferrite/Austenite Transformations in Duplex Stainless Steel Weldments Using Synchrotron Radiation," *Sci. Tech. Weld. Join*., 7(3) (2002), 159-171.

2. W. Zhang, G.G. Roy, J.W. Elmer, and T. DebRoy, "Modeling of Heat Transfer and Fluid Flow During Gas Tungsten Arc Spot Welding of Low Carbon Steel," *J. Appl. Phys*., 93(5) (2003), 3022-3033.

3. L. Karlsson, "Intermetallic Phase Precipitation in Duplex Stainless Steels and Weld Metals: Metallurgy, Influence on Properties, Welding and Testing Aspects," WRC Bulletin 438, January 1999.

4. J.-O. Nilsson, "Super Duplex Stainless Steels," *Mater Sci and Technol*, 8 (1992), 685-700.

5. J.-O. Nilsson, L. Karlsson, and J.-O. Andersson, "Secondary Austenite Formation and its Relation to Pitting Corrosion in Duplex Stainless Steel Weld Metal," *Mater Sci and Technol*, 11 (1995), 276-283.

6. J.-O. Nilsson, et al., "Structural Stability of Super Duplex Stainless Weld Metals and Its Dependence on Tungsten and Copper," *Metall Mater Trans A*, 27A (1996), 2196-2208.

7. Y.S. Ahn, J.M. Kim, and B.H. Jeong, "Effect of Aging Treatments and Microstructural Evolution on Corrosion Resistance of Tungsten Substituted 2205 Duplex Stainless Steel," *Mater Sci and Technol*, 18 (2002), 383-388.

8. J.-O. Nilsson and A. Wilson, "Influence of Isothermal Phase Transformation on Toughness and Pitting Corrosion of Super Duplex Stainless Steel SAF 2507," *Mater Sci and Technol*, 9 (1993), 545-554.

9. Y.S. Ahn and J.P. Kang, "Effect of Aging Treatments on Microstructure and ImpacT Properties of Tungsten Substituted 2205 Duplex Stainless Steel," *Mater Sci and Technol*, 16 (2000), 382-388.

10. P.D. Southwick and R.W.K. Honeycombe, "Decomposition of Ferrite to Austenite in 26%CR-5%Ni Stainless Steel,"*Metal Sci*, 14 (1980), 253-261.

11. V. Karpenko, et al., "Beamline 10 – A Multipole Wiggler Beamline at SSRL," *Rev. Sci. Instrum*., 60 (1989), 1451-1460.

12. J.W. Elmer, et al., "Analysis of Heat-Affected Zone Phase Transformations Using In-Situ Spatially Resolved X-Ray Diffraction with Synchrotron Radiation," *Metall. Mater. Trans. A*, 27A (1996), 775-83.

13. J. Wong, et al., "In-Situ Phase Mapping and Transformation Study in Fusion Welds," *J. Mat. Sci*., 32 (1997), 1493-1500.

14. J.W. Elmer, J. Wong, and T. Ressler, Spatially Resolved X-Ray Diffraction Phase Mapping and Alpha→Beta→Alpha Transformation Kinetics in the Heat-Affected Zone of Commercially Pure Titanium Arc Welds," *Metall. Mater. Trans. A*, 29A (1998), 2761-2773.

15. T. Ressler, J. Wong, and J.W. Elmer, "Investigation of Real-Time Microstructure Evolution in Steep Thermal Gradients Using In-Situ Spatially Resolved X-Ray Diffraction: A Case Study for Ti Fusion Welds," *J. Phys. Chem. B*, 102 (1998), 10724-10735.

16. Z. Yang, J.W. Elmer, J. Wong, and T. DebRoy, "Evolution of Titanium Arc Weldment Macro and Microstructures – Modeling and Real Time Mapping of Phases," *Weld J.*, 79(4) (2000), 97s–111s.

17. J.W. Elmer, J. Wong, and T. Ressler, "Spatially Resolved X-Ray Diffraction Mapping of Phase Transformations in the Heat-Affected Zone of Carbon-Manganese Steel Arc Welds," *Metall. Mater. Trans. A*, 32A (2001), 1175-1188.

18. J.W. Elmer, J. Wong, and T. Ressler, "In-Situ Observations of Phase Transformations During Solidification and Cooling of Austenitic Stainless Steel Welds Using Time-Resolved X-Ray Diffraction," *Scripta Mater*, 43(8) (2000), 751-757

19. *PowderCell, v. 1.0*, Federal Institute for Materials Research and Testing, Rudower Chaussee 5, 12489 Berlin, Germany.

20. W. Zhang, J.W. Elmer, and T. DebRoy, "Kinetics of Ferrite to Austenite Transformation During Welding of 1005 Steel," *Scripta Mater*, 46 (2002), 753-757.

21. W. Zhang, J.W. Elmer, and T. DebRoy, "Modeling and Real Time Mapping of Phases during GTA Welding of 1005 Steel," *Mater Sci Eng A*, 333(1-2) (2002), 320-335.

22. E.A. Brandes, ed., *Smithells Metals Reference Book*, 7th Edition, (London: Butterworth and Heinemann, 1992).

23. M.W. Chase, Jr., *et al*., *JANAF Thermochemical Tables*, 3rd Edition, (Washington, DC: American Chemical Society and American institute for Physics, 1985).

24. B.D. Cullity and S.R. Stock, *Elements of X-Ray Diffraction*, 3rd Edition, (Prentice Hall, Upper Saddle River, NJ, 2001).

25. T.A. Palmer, et al., "Investigation of the Kinetics of the Ferrite/Austenite Phase Transformation in the HAZ of a 2205 Duplex Stainless Steel Weldment," *Trends in Welding Research*, ed. by S.A. David, T. DebRoy, J.C. Lippold, H.B. Smartt, and J.M. Vitek, (Materials Park, OH: ASM International, 2003), 23-28.

26. A. Engström, L. Höglund, and J. Ågren, "Computer Simulation of Diffusion in Multi-phase Systems," *Metall. Mater. Trans. A.,* 25A (1994), 1127-1134

27. E. Kozeschnik and B. Buchmayr, "MATCALC-A Simulation Tool for Multicomponent Thermodynamics, Diffusion and Phase Transformations," *Mathematical Modeling of Weld Phenomena 5*, ed. H. Cerjak, (London: Institute of Materials, 2001), 349-361